



HAL
open science

Quantum-tunneling isotope-exchange reaction $\text{H}_2 + \text{D}^- \rightarrow \text{HD} + \text{H}^-$

Chi Hong Yuen, Mehdi Ayouz, Eric S Endres, Olga Lakhamanskaya, Roland Wester, Viatcheslav Kokoouline

► **To cite this version:**

Chi Hong Yuen, Mehdi Ayouz, Eric S Endres, Olga Lakhamanskaya, Roland Wester, et al.. Quantum-tunneling isotope-exchange reaction $\text{H}_2 + \text{D}^- \rightarrow \text{HD} + \text{H}^-$. *Physical Review A: Atomic, molecular, and optical physics* [1990-2015], 2018, 97 (2), pp.22705 - 22705. 10.1103/PhysRevA.97.022705 . hal-01820456

HAL Id: hal-01820456

<https://hal.science/hal-01820456>

Submitted on 21 Jun 2018

HAL is a multi-disciplinary open access archive for the deposit and dissemination of scientific research documents, whether they are published or not. The documents may come from teaching and research institutions in France or abroad, or from public or private research centers.

L'archive ouverte pluridisciplinaire **HAL**, est destinée au dépôt et à la diffusion de documents scientifiques de niveau recherche, publiés ou non, émanant des établissements d'enseignement et de recherche français ou étrangers, des laboratoires publics ou privés.

Quantum-tunneling isotope-exchange reaction $\text{H}_2 + \text{D}^- \rightarrow \text{HD} + \text{H}^-$ Chi Hong Yuen,¹ Mehdi Ayouz,² Eric S. Endres,³ Olga Lakhmanskaya,³ Roland Wester,³ and Viatcheslav Kokoouline¹¹*Department of Physics, University of Central Florida, Orlando, Florida 32816, USA*²*Laboratoire de Genie des Procédés et des Matériaux, Ecole Centrale Paris, CentraleSupélec, Campus de Chatenay-Malabry Grande Voie des Vignes, F-92 295 Chatenay-Malabry Cedex, France*³*Institut für Ionenphysik und Angewandte Physik, Universität Innsbruck, Technikerstraße 25, 6020 Innsbruck, Austria*

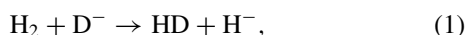
(Received 18 October 2017; published 20 February 2018; corrected 4 May 2018)

The tunneling reaction $\text{H}_2 + \text{D}^- \rightarrow \text{HD} + \text{H}^-$ was studied in a recent experimental work at low temperatures (10, 19, and 23 K) by Endres *et al.* [*Phys. Rev. A* **95**, 022706 (2017)]. An upper limit of the rate coefficient was found to be about 10^{-18} cm³/s. In the present study, reaction probabilities are determined using the ABC program developed by Skouteris *et al.* [*Comput. Phys. Commun.* **133**, 128 (2000)]. The probabilities for ortho- H_2 and para- H_2 in their ground rovibrational states are obtained numerically at collision energies above 50 meV with the total angular momentum $J = 0-15$ and extrapolated below 50 meV using a WKB approach. Thermally averaged rate coefficients for ortho- and para- H_2 are obtained; the largest one, for ortho- H_2 , is about 3.1×10^{-20} cm³/s, which agrees with the experimental results.

DOI: [10.1103/PhysRevA.97.022705](https://doi.org/10.1103/PhysRevA.97.022705)**I. INTRODUCTION**

In the interstellar medium (ISM), the H^- ion could be responsible for the formation of molecular anions, several of which have recently been observed [1–9]. For example, the CN^- ion [9] could be formed in the reaction $\text{H}^- + \text{HCN} \rightarrow \text{H}_2 + \text{CN}^-$ [10,11]. However, H^- has never been observed in the ISM by photoabsorption spectroscopy. Its detection is difficult because it has only one bound electronic state. A few unsuccessful efforts were made to search for it in the ISM, such as using far-ultraviolet autodetachment transitions [12]. The existence of H^- can also be inferred indirectly via the spectroscopy of the H_3^- ion, which could be formed by radiative association of H_2 and H^- in diffuse molecular clouds [13].

For an eventual indirect detection of H^- in the ISM via detection of H_3^- , studying the structure and formation of the H_3^- system with its isotopologues is important [13,14]. Recently, reactive scattering of the D^- ion in collisions with H_2 ,



was studied in an experiment by Endres *et al.* [15]. This exothermic reaction has a reaction barrier of 330 ± 60 meV [16], which cannot be overcome by thermal activation at low temperatures. Therefore, at low temperatures in cold molecular clouds in the ISM, the reaction can proceed only by quantum tunneling and cannot be described with the classical Langevin theory. As H_2D^- is one of the simplest anionic triatomic molecules, the reaction could serve as a benchmark process for quantum tunneling at low temperatures. The experiment of Ref. [15] was performed in a cryogenic 22-pole ion trap. From D^- loss-rate measurements, it was concluded that the upper limit of the rate coefficient at 10 K is 2.6×10^{-18} cm³/s. The absence of the H^- signal gave a smaller upper limit of 9×10^{-19} cm³/s.

There have been several theoretical investigations of the reaction (1). However, the majority of the studies considered

collision energies from about 0.3 to 2 eV. For example, a time-dependent wave-packet method with and without Coriolis coupling was used in Refs. [17,18] and a quasiclassical trajectory method was used in Ref. [19]. The cross section for the process using both a time-dependent and time-independent method was reported by Giri and Sathyamurthy [20]. A comparison of reaction cross sections obtained using different available potential-energy surfaces was made at collision energies above 0.3 eV in Ref. [21]. There is also a study using the variational transition-state method, which gave the rate coefficient of the order of 10^{-23} cm³/s at 30 K [22]. At ultracold and cold temperatures, a similar reaction $\text{H}_2(v=0-5, j=0,1) + \text{D} \rightarrow \text{HD} + \text{H}$ was reported by Simbotin and Côté [23]. Giri and Sathyamurthy have also reported [24] theoretical results for the $\text{H}^- + \text{HD}$ collisions with the HD molecule being in the first excited vibrational level. The present study is focused on a quantum mechanical approach to obtain the cross section of reaction (1) at low energies, below the potential barrier.

II. THEORETICAL APPROACH

In this study, we employ the H_3^- potential-energy surface (PES) calculated by Ayouz *et al.* [14]. The PES has a barrier of about 450 meV above the dissociation limit of $\text{H}^- + \text{H}_2$, when H_2 is at the equilibrium geometry, along the minimum-energy pathway of the reaction (1) (see Fig. 1). The barrier is about two orders of magnitude larger than a typical collision energy at 10 K in the experiment by Endres *et al.* [15]. Therefore, the reactive scattering is highly suppressed at 10 K. Figure 2 shows the hyperspherical adiabatic (HSA) energy curves of H_2D^- as a function of the hyper-radius (for details, see Ref. [25]). As Fig. 2 demonstrates, at low energies of collisions between D^- and the H_2 molecule in the rotational level $j=0$ or 1, the possible reaction channels are $\text{H}^- + \text{HD}$ with HD being in the rotational state $j=0, 1$, or 2.

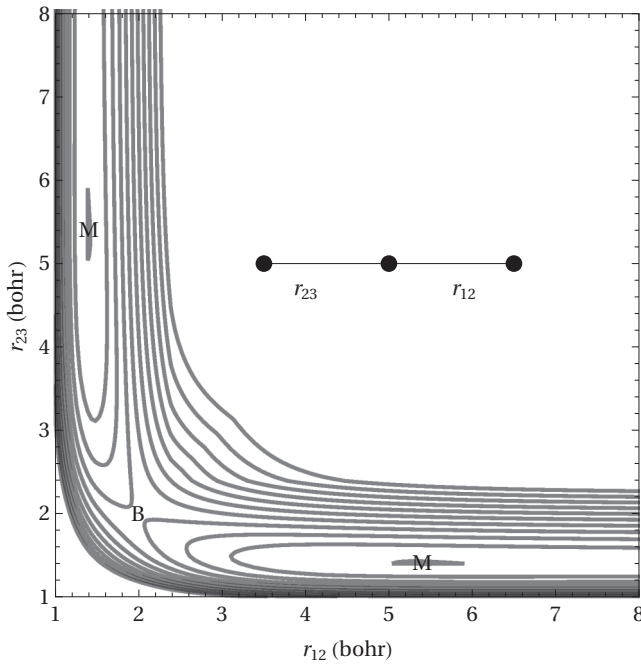


FIG. 1. $\text{H}_3^-/\text{H}_2\text{D}^-$ PES as a function of two internuclear distances r_{12} and r_{23} for linear geometries. The absolute energy minimum of the PES is indicated with M and the peak of the potential barrier is labeled with B. Successive energy contours differ by 0.16 eV.

At low collision energies, the reaction probability is extremely small, which requires a theoretical approach able to provide the required accuracy for the probabilities. To assess and compare the accuracy of different numerical methods, we have performed a restricted calculation of the reaction probabilities for parahydrogen in the ground rovibrational state with the total angular momentum $J = 0$ using three different approaches: the time-independent hyperspherical adiabatic approach [26], the multiconfiguration time-dependent Hartree

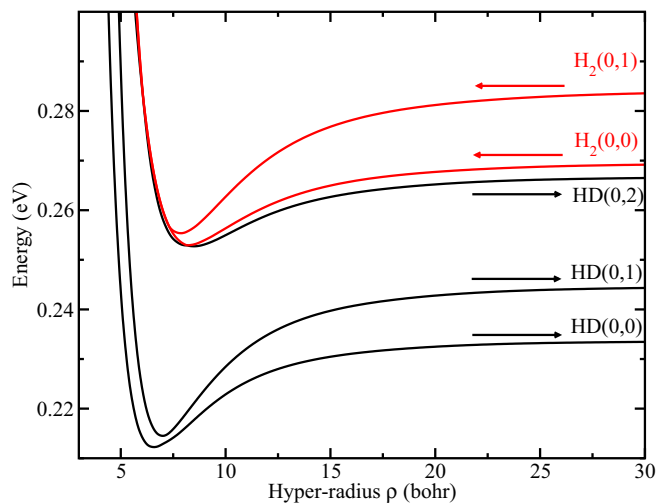


FIG. 2. Hyperspherical adiabatic potential-energy curves for H_2D^- . At low collision energies between $\text{H}_2(v = 0, j = 0, 1)$ and D^- , there are three open exit channels for $\text{HD}(v, j)$ with $v = 0$ and $j = 0, 1, 2$ [25].

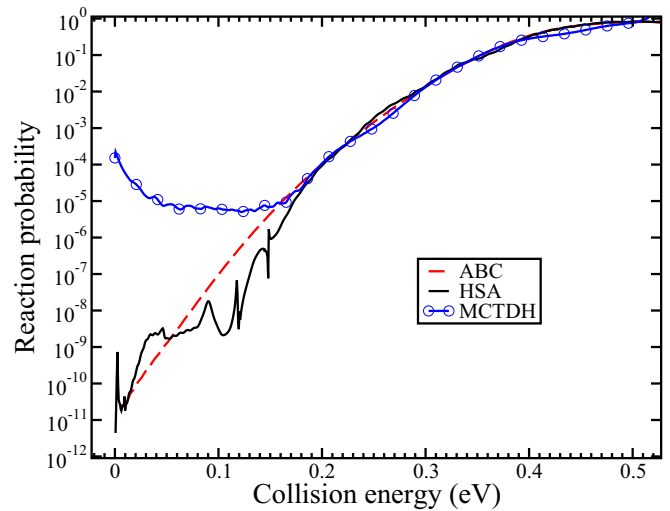


FIG. 3. Reaction probabilities of the reaction $\text{H}_2(0,0) + \text{D}^- \rightarrow \text{HD} + \text{H}^-$ with the total angular momentum $J = 0$, obtained from the HSA approach (black solid curve), the MCTDH method (blue solid curve with circles), and the ABC program (red dashed curve).

(MCTDH) method [27], and the ABC program [28]. Only a brief overview of the three methods is provided below; details can be found in [26–28] and the references therein.

The HSA approach represents different arrangements of the system by using a single set of hyperspherical coordinates. As a first step in this method, one calculates HSA energies and wave functions at many fixed hyper-radii. At large values of the hyper-radius, the energies and wave functions represent the rovibrational states of the dimer, as shown in Fig. 2. The nonadiabatic couplings between the HSA channels are represented using the modified slow variable discretization [29]. Using the eigenchannel R -matrix approach, the scattering matrix is extracted at the last grid point of the hyper-radius without performing a coordinate transformation, as is performed in Refs. [30,31]. The MCTDH method is a general algorithm for solving the time-dependent Schrödinger equation for multidimensional systems. It has been successful in treating reactive scattering for different systems [32,33]. This method propagates the incoming wave packet along the PES. The outgoing flux is absorbed by placing a complex absorbing potential at the reaction coordinate, and the reaction probability is extracted from the outgoing flux. The ABC program is also able to represent the reactive scattering of a dimer and an atom. It has been successfully applied to many three-body systems [23,34,35]. It is based on solving the Schrödinger equation using the coupled-channel approach in Delves hyperspherical coordinates. The coupled-channel basis functions are constructed on the surface of the hypersphere at each hyper-radius. Finally, the parity-adapted scattering matrix is obtained by applying boundary conditions.

Figure 3 compares the results obtained using the three methods. At collision energies above 0.2 eV, the reaction probabilities from all three methods are in good agreement. Below that energy, in the tunneling regime, the results diverge. In the MCTDH calculation below 0.1 eV, the outgoing flux is extremely small, which sets a limit on accuracy of the calculation. To achieve a better accuracy in the MCTDH

approach, one needs to significantly increase the propagation time and the length of the grid, which makes the calculation much more expensive compared to the ABC method. In the spectrum of the $\text{H}_2 + \text{D}^-$ collisions, one expects to observe rovibrational resonances similar to the ones computed in Ref. [25]. Such resonances are situated at collision energies above 25 meV. Indeed, in the HSA spectrum shown in Fig. 3, the peaks at energies about 0.1 and 0.15 eV correspond to the two series of resonances predicted in [25]. At energies below 0.1 eV, the HSA results show the oscillations that do not correspond to any resonance. These are artifacts of the present HSA method, which is currently unable to represent very small tunneling probabilities below 0.1 eV. A disadvantage of the ABC program is that it does not represent rovibrational Feshbach resonances due to the restricted basis of coupled-channel functions employed in the approach. Because we are interested only in the thermally averaged rate coefficient at temperature about 10 K, the resonance structures at higher collision energies are irrelevant. Therefore, numerical stability of the method at low energies is the most important factor. At energies below 0.1 eV, the ABC program produced smooth reaction probability as expected since there is no resonance present in this region. Therefore, the ABC program was chosen to perform calculations for all values of J needed to be included in the study.

In the ABC program, the total reaction cross section is obtained as

$$\sigma_{\lambda' \leftarrow \lambda v j}^P(E_i) = \frac{\pi}{k_i^2} \sum_J (2J+1) P_J(E_i),$$

$$P_J(E_i) = \frac{1}{2j+1} \sum_{v' j'} \sum_{k'} \sum_k |S_{\lambda' v' j' k' \leftarrow \lambda v j k}^{J,P}|^2, \quad (2)$$

where E_i is the collision energy; $k_i = \sqrt{2\mu E_i}/\hbar$, with μ being the reduced mass of the D^- ion and the H_2 molecule; λ and λ' are the initial, $\text{H}_2 + \text{D}^-$, and the final, $\text{HD} + \text{H}^-$, rearrangements correspondingly; J and k are the total angular momentum and its projection on a fixed axis in the molecular reference frame; v, j and v', j' are the initial and final rovibrational levels of the H_2 and HD molecules, respectively; and P is the parity quantum number. In the above equation, P_J has a meaning of the reaction probability for given values of J, λ, λ', v , and j .

At collision energies above 50 meV, the cross section converges when channels with energies up to 2.3 eV above the dissociation limit and 16 or 17 rotational states for para- or ortho- H_2 are included. A grid along hyper-radius ρ until 20 bohrs with a grid step of $\Delta\rho = 0.08$ bohrs was used in the calculation. The largest value of the quantum number k is 4. At energies below 50 meV, convergence with respect to the number of channels is poor because of the difficulty to represent the very small reaction probability. To extend the converged results obtained at energies above 50 meV into the low-energy region, a WKB approach can be used. Although the tunneling through the potential barrier occurs in the three-dimensional space of internuclear distances of H_2D^- , for the purpose of using a simplified WKB approach to extrapolate the numerical results below 50 meV, we introduce a generalized tunneling coordinate x , which could approximately be viewed as a minimum-energy-path coordinate. Therefore, the WKB

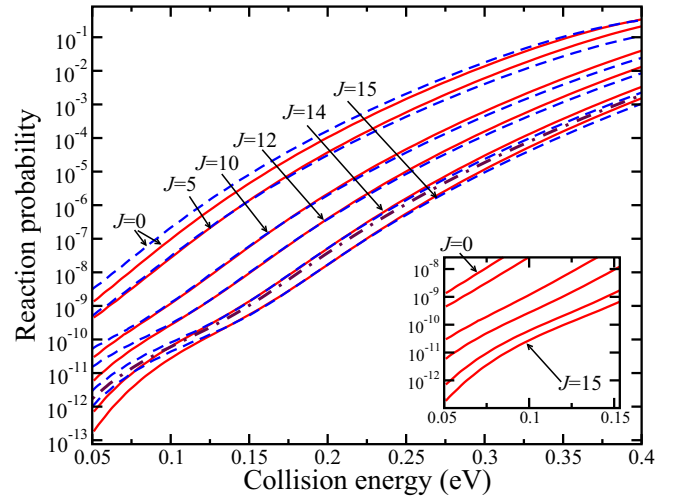


FIG. 4. The dashed lines and the solid lines show the reaction probability of ortho- H_2 [with $P = (-1)^J$] and para- H_2 in their ground rovibrational states $j = 1$ and 0 for the total angular momentum $J = 0, 5, 10, 12, 14$, and 15. The probabilities decrease with J . The dash-dotted line shows the reaction probability of ortho- H_2 with $J = 1$ and $P = 1$. The inset shows only the para- H_2 curves from the main graph to illustrate the effect of the increasing J on the reaction probability.

formula

$$P_{J=0}(E_i) \sim \exp\left\{-\frac{2}{\hbar} \int_{w_1}^{w_2} \sqrt{2\mu[V(x) - E_i]} dx\right\} \quad (3)$$

for the tunneling probability is used, where w_1 and w_2 are two turning points along x .

In the Appendix, we show that at small E_i , the J dependence of the probability behaves as

$$P_J(E_i) \approx P_{J=0}(E_i) \exp[-\lambda J(J+1)]. \quad (4)$$

The sum of reaction probabilities can then be expressed as

$$\sum_J (2J+1) P_J \approx P_{J=0} \sum_J (2J+1) \exp[-\lambda J(J+1)]$$

$$\approx \exp[AE_i^2 + BE_i + C], \quad (5)$$

where A, B , and C are some constant obtained by fitting the result from the ABC program at collision energies between 50 and 80 meV to the WKB formula.

III. RESULTS AND DISCUSSION

Figure 4 shows the reaction probabilities obtained by solving the Schrödinger equation numerically for ortho- H_2 and para- H_2 in their ground rovibrational states $j = 1$ and 0, correspondingly, for different total angular momenta J as a function of collision energy. For ortho- H_2 with the total parity $P = (-1)^{J+1}$, only the $k = 1$ channel can contribute to the reaction. However, the reaction probability for $k = 1$ is about three orders of magnitude smaller than for the channel with $P = (-1)^J$ and $k = 0$ at $J = 1$. Because the ground-state energy for ortho- H_2 is about 15 meV higher than for para- H_2 , the effective reaction barrier for ortho- H_2 is lower and, therefore, its reaction probability is larger at low collision energies, as it is evident in Fig. 4. At higher collision

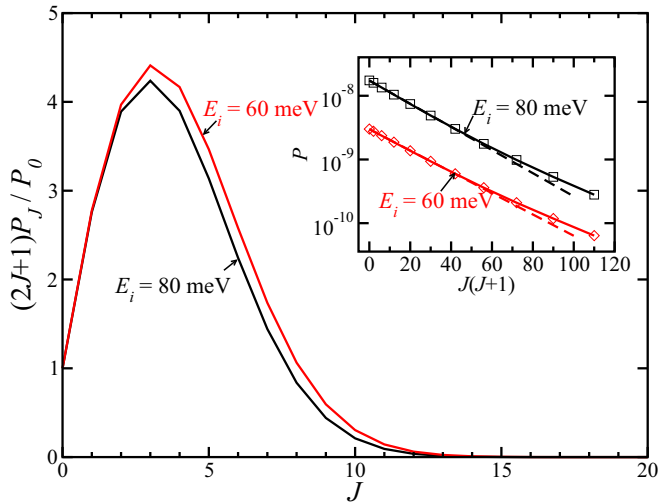


FIG. 5. The figure shows the ratio of $(2J + 1)P_J/P_{J=0}$ as a function of J for collision energies $E_i = 60$ and 80 meV for para- H_2 . The inset shows the reaction probability at fixed energies of 60 meV [red (gray) diamonds] and 80 meV (black squares) as a function of $J(J + 1)$. The dashed lines of the same color in the inset are the linear fit according to Eq. (4).

energies, the difference between the ground-state energies is insignificant and the probabilities are almost equal. But due to the threefold degeneracy in the entrance channel for ortho- H_2 , the overall reaction probability for para- H_2 is somewhat larger than for ortho- H_2 at higher collision energies.

At low collision energies, only small values J of the total angular momentum contribute to the total reaction probability as Eq. (4) suggests. The numerical calculations confirm it: The inset of Fig. 5 shows that at collision energies of 60 and 80 meV, the reaction probability for para- H_2 indeed follows the trend of Eq. (4). The main graph of Fig. 5 shows the ratio $(2J + 1)P_J/P_{J=0}$ for different J . The degeneracy factor $2J + 1$ was included in the ratio because it increases the relative contribution of a particular J into the total cross section. The figure demonstrates that $J = 3$ contributes the most to the reaction, while for $J > 10$ the contributions to the sum of reaction probabilities are small.

Figure 6 shows the the sum of reaction probabilities $\sum(2J + 1)P_J$ for ortho- and para- H_2 as a function of the collision energy. The values of $J = 0$ – 15 were included in the sum. In order to extrapolate to the low-energy region, we fit the curves obtained numerically to Eq. (5) using the data points for energies between 50 and 80 meV. The uncertainty associated with the fit is within 2% , which justifies the approximation made in the derivation of Eq. (5). Furthermore, because the PES has a barrier of 450 meV and due to the H_2 zero-point energy of about 270 meV in the asymptotic $H_2 + D^-$ region, the effective reaction barrier is lowered to about 180 meV. As the figure indicates, the sum of reaction probabilities becomes significant around that energy and above.

Extrapolated to the low-energy region, the thermally averaged rate coefficient is computed using Eq. (2), with the results shown in Fig. 7. The rate coefficients for ortho- and para- H_2 are about 3.1×10^{-20} and 1.2×10^{-20} cm^3/s , respectively, at temperatures 10 – 30 K. The difference between ortho- and para- H_2

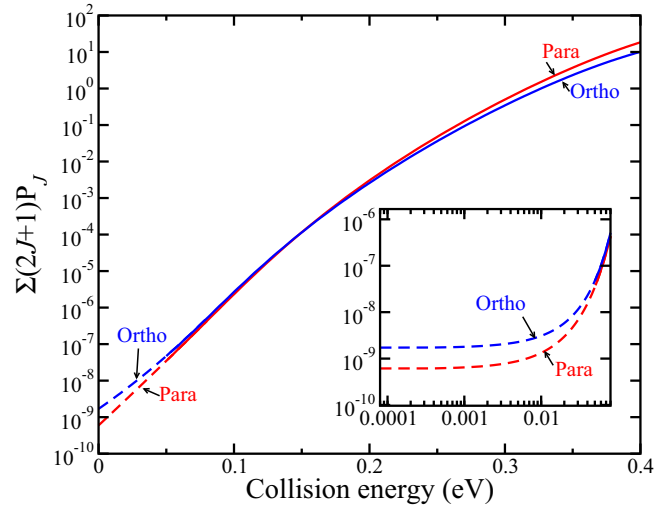


FIG. 6. The figure shows the sum of reaction probabilities $\sum(2J + 1)P_J$ for ortho- H_2 and para- H_2 (solid lines) as a function of the collision energy. The dashed lines of the same color are the fit to the WKB formula of Eq. (5). The uncertainty is within 2% . The inset is a zoom of the curves in the low-energy region.

values at low temperatures is explained by the difference in the ground-state energy and, as a result, by a smaller effective potential barrier for ortho- H_2 . The thermally averaged rate coefficient for normal hydrogen is closer to ortho- H_2 because ortho- H_2 has a three-times-larger statistical weight compared to the para- H_2 . Therefore, our result is consistent with the experimental upper limit obtained by Endres *et al.*

IV. CONCLUDING REMARKS

In the study, the thermally averaged rate coefficient for the nuclei exchange reaction $H_2 + D^- \rightarrow HD + H^-$ was computed for temperatures up to 400 K. In the calculation, the

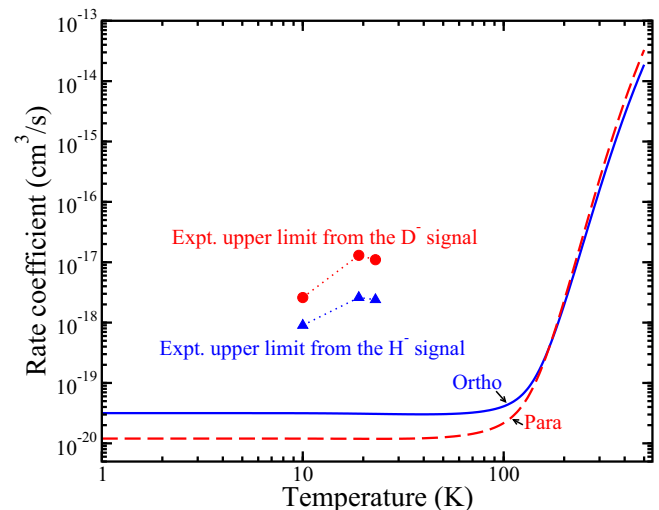


FIG. 7. Thermally averaged rate coefficient for ortho- H_2 and para- H_2 as a function of temperature. The circles and triangles represent the experimental upper limits obtained from the D^- signal and from the H^- signal at 10 , 19 , and 23 K [15].

accurate PES [14] of the system and the ABC code for reactive quantum scattering [28] were used. At low collision energies, a WKB approach was used to extrapolate the results of the fully quantum approach.

The obtained thermally averaged rate coefficient for ortho- H_2 is about three times larger than for para- H_2 at temperatures below 80 K, while at higher temperatures the coefficients become almost equal. The present theoretical results are about ten times smaller than the experimental upper limit [15], suggesting that a further improvement of the sensitivity of the signal in the experiment may lead to the observation of the H^- ions produced from this reaction. Also, the present results suggest that an experiment performed at different temperatures should reveal a strong temperature dependence of the tunneling probabilities at temperatures 70–300 K.

Future experiments studying collisions of H_2 with the H^- isotopes may help to eventually detect the H^- ion in the interstellar space. The ion cannot be detected directly by the absorption or emission spectroscopy, but in collisions with H_2 it may form the loosely bound H_3^- molecule. If detected, H_3^- could serve as a precursor for H^- . The most likely process to form H_3^- is the three-body collisions involving H_2 , H^- , and a third atom or molecule. In the interstellar space, the third body could be another H_2 molecule; in the laboratory, it could be a buffer gas species, such as helium. Therefore, further experiments studying collisions of H_2 and H^- are highly desirable.

ACKNOWLEDGMENTS

This work is supported by the National Science Foundation Grant No. PHY-15-06391 and the Chateaubriand Fellowship of the Office for Science and Technology of the Embassy of France in the United States. V.K. also acknowledges financial support from the Austrian-American Educational Commission. R.W. acknowledges support by the Austrian Science Fund (FWF) through Project No. I2920-N27. E.S.E. acknowledges support from the Fonds National de la Recherche Luxembourg (Grant No. 6019121).

APPENDIX: EXTRAPOLATION USING A WKB APPROACH

In this appendix, we derive Eqs. (4) and (5) and justify the approximations made above. For collision energies much smaller than the potential barrier, the probability can be expanded in powers of small E_i ,

$$P_{J=0}(E_i) \approx \exp[aE_i^2 + bE_i + c], \quad (\text{A1})$$

with

$$a = \frac{\sqrt{2\mu}}{4\hbar} \int_{w_1}^{w_2} \frac{1}{V(x)^{3/2}} dx, \quad b = \frac{\sqrt{2\mu}}{\hbar} \int_{w_1}^{w_2} \frac{1}{\sqrt{V(x)}} dx, \\ c = -\frac{2\sqrt{2\mu}}{\hbar} \int_{w_1}^{w_2} \sqrt{V(x)} dx,$$

where $V(x)$ is the potential barrier. We assume that at $x = 0$, the potential barrier reaches its peak. The quantities a, b , and c depend on energy implicitly. To include their energy dependence in Eq. (A1), one can again expand them in powers of small E_i . Because the potential barrier is a very steep

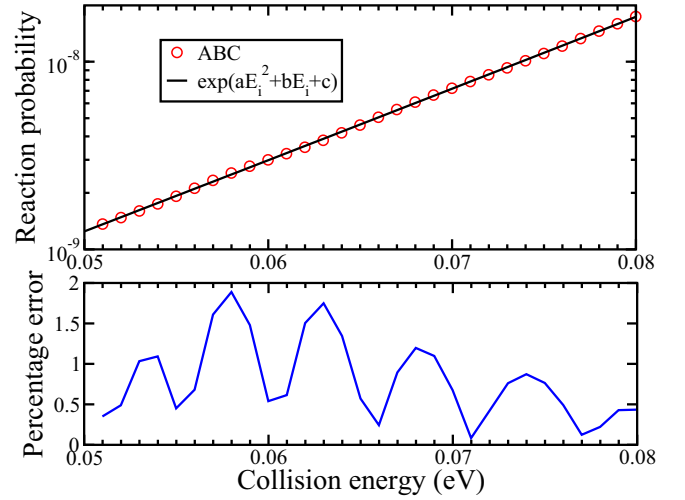


FIG. 8. The upper panel shows the reaction probability of $\text{H}_2(0,0)$ with the total angular momentum $J = 0$ obtained from the fully quantum approach and the WKB formula of Eq. (A1). The lower panel shows the difference between the two curves in the upper panel.

function of x , increasing the collision energy E_i slightly decreases the width of the barrier, i.e., brings the turning points w_1 and w_2 closer to each other. It means that a, b , and $-c$ are positive quantities, decreasing slowly with E_i if the energies are much smaller than the effective potential barrier of about 180 meV. The matching between the WKB and fully quantum results is performed near 50–80 meV. To evaluate the uncertainty of the fit, the simple case of $\text{H}_2(0,0)$ with the total angular momentum $J = 0$ was considered. Figure 8 shows the fit using Eq. (A1). The lower panel of the figure demonstrates that the difference between the fit and the fully quantum result is about 2% or less, which justifies the validity of the WKB extrapolation.

To account for the dependence of the probability on the total angular momentum J , we note that the centrifugal energy $B(x)J(J+1)$ at the top of the barrier at $x = 0$ with $B(0) \sim 0.1$ meV at low J (≤ 6) is much smaller than the potential barrier itself. Therefore, we can simply change E_i to $E_i - B(x)J(J+1)$ in Eq. (A1). At $E_i = 80$ meV, E_i is about ten times or more larger than the centrifugal energy. Therefore, the larger contribution from the J dependence of the probability can be accounted for as

$$P_J(E_i) \approx P_{J=0}(E_i) \exp[-\lambda J(J+1)], \\ \lambda = \frac{\sqrt{2\mu}}{\hbar} \int_{w_1}^{w_2} \frac{B(x)}{\sqrt{V(x)}} dx. \quad (\text{A2})$$

For large J , the above approximation is not accurate because the centrifugal barrier is significant, but the reaction probabilities are small for $J > 6$ (see Figs. 4 and 5). Finally, the sum of reaction probabilities can be expressed as

$$\sum_J (2J+1) P_J \approx P_{J=0} \sum_J (2J+1) \exp[-\lambda J(J+1)] \\ \approx \exp[AE_i^2 + BE_i + C], \quad (\text{A3})$$

where we combined exponents in $\exp[-\lambda J(J+1)]$ and $P_{J=0}$, and introduced new constants A, B , and C .

- [1] M. C. McCarthy, C. A. Gottlieb, H. Gupta, and P. Thaddeus, *Astrophys. J. Lett.* **652**, L141 (2006).
- [2] H. Gupta, S. Brünken, F. Tamassia, C. A. Gottlieb, M. C. McCarthy, and P. Thaddeus, *Astrophys. J. Lett.* **655**, L57 (2007).
- [3] K. Kentarou, R. Fujimori, S. Aimi, S. Takano, E. Okabayashi, H. Gupta, S. Brünken, C. Gottlieb, M. McCarthy, and P. Thaddeus, *Publ. Astron. Soc. Jpn.* **59**, L47 (2007).
- [4] J. Cernicharo, M. Guélin, M. Agúndez, K. Kawaguchi, M. McCarthy, and P. Thaddeus, *Astron. Astrophys.* **467**, L37 (2007).
- [5] J. Cernicharo, M. Guélin, M. Agúndez, M. C. McCarthy, and P. Thaddeus, *Astrophys. J. Lett.* **688**, L83 (2008).
- [6] P. Thaddeus, C. A. Gottlieb, H. Gupta, S. Brunken, M. C. McCarthy, M. Agundez, M. Guelin, and J. Cernicharo, *Astrophys. J.* **677**, 1132 (2008).
- [7] E. Herbst and Y. Osamura, *Astrophys. J.* **679**, 1670 (2008).
- [8] N. Harada and E. Herbst, *Astrophys. J.* **685**, 272 (2008).
- [9] M. Agúndez, J. Cernicharo, M. Guélin, C. Kahane, E. Roueff, J. Klos, F. Aoi, F. Lique, N. Marcelino, J. Goicoechea, M. González García, C. Gottlieb, M. McCarthy, and P. Thaddeus, *Astron. Astrophys.* **517**, L2 (2010).
- [10] N. Douguet, S. Fonseca dos Santos, M. Raoult, O. Dulieu, A. E. Orel, and V. Kokoouline, *Phys. Rev. A* **88**, 052710 (2013).
- [11] M. Satta, F. Gianturco, F. Carelli, and R. Wester, *Astrophys. J.* **799**, 228 (2015).
- [12] T. Ross, E. J. Baker, T. P. Snow, J. D. Destree, B. L. Rachford, M. M. Drosback, and A. G. Jensen, *Astrophys. J.* **684**, 358 (2008).
- [13] M. Ayouz, R. Lopes, M. Raoult, O. Dulieu, and V. Kokoouline, *Phys. Rev. A* **83**, 052712 (2011).
- [14] M. Ayouz, O. Dulieu, R. Guérout, J. Robert, and V. Kokoouline, *J. Chem. Phys.* **132**, 194309 (2010).
- [15] E. S. Endres, O. Lakhmanskaya, M. Simpson, S. Spieler, and R. Wester, *Phys. Rev. A* **95**, 022706 (2017).
- [16] E. Haufler, S. Schlemmer, and D. Gerlich, *J. Phys. Chem.* **101**, 6441 (1997).
- [17] C. Morari and R. Jaquet, *J. Phys. Chem. A* **109**, 3396 (2005).
- [18] L. Yao, L. Ju, T. Chu, and K.-L. Han, *Phys. Rev. A* **74**, 062715 (2006).
- [19] W. Zhang, Y. Liu, and X. He, *Chem. Phys. Lett.* **489**, 237 (2010).
- [20] K. Giri and N. Sathyamurthy, *J. Phys. Chem. A* **110**, 13843 (2006).
- [21] D. Wang and R. Jaquet, *J. Phys. Chem. A* **117**, 7492 (2013).
- [22] H. Luo, Y. Wu, and L. Ju, *Comp. Theor. Chem.* **963**, 475 (2011).
- [23] I. Simbotin and R. Côté, *New J. Phys.* **17**, 065003 (2015).
- [24] K. Giri and N. Sathyamurthy, *Chem. Phys. Lett.* **444**, 23 (2007).
- [25] M. Ayouz, O. Dulieu, and J. Robert, *J. Phys. Chem. A* **117**, 9941 (2013).
- [26] C. H. Yuen and V. Kokoouline, *Europhys. J. D* **71**, 19 (2017).
- [27] M. H. Beck, A. Jäckle, G. Worth, and H.-D. Meyer, *Phys. Rep.* **324**, 1 (2000).
- [28] D. Skouteris, J. Castillo, and D. Manolopoulos, *Comput. Phys. Commun.* **133**, 128 (2000).
- [29] O. I. Tolstikhin, S. Watanabe, and M. Matsuzawa, *J. Phys. B: At. Mol. Opt. Phys.* **29**, L389 (1996).
- [30] R. T. Pack and G. A. Parker, *J. Chem. Phys.* **87**, 3888 (1987).
- [31] J. Launay and M. Le Dourneuf, *Chem. Phys. Lett.* **163**, 178 (1989).
- [32] S. Sukiasyan and H.-D. Meyer, *J. Phys. Chem. A* **105**, 2604 (2001).
- [33] T. Wu, H.-J. Werner, and U. Manthe, *Science* **306**, 2227 (2004).
- [34] N. Balakrishnan and A. Dalgarno, *Chem. Phys. Lett.* **341**, 652 (2001).
- [35] E. Bodo, F. Gianturco, and A. Dalgarno, *J. Chem. Phys.* **116**, 9222 (2002).

Correction: The surname of the fourth author contained an error and has been corrected.